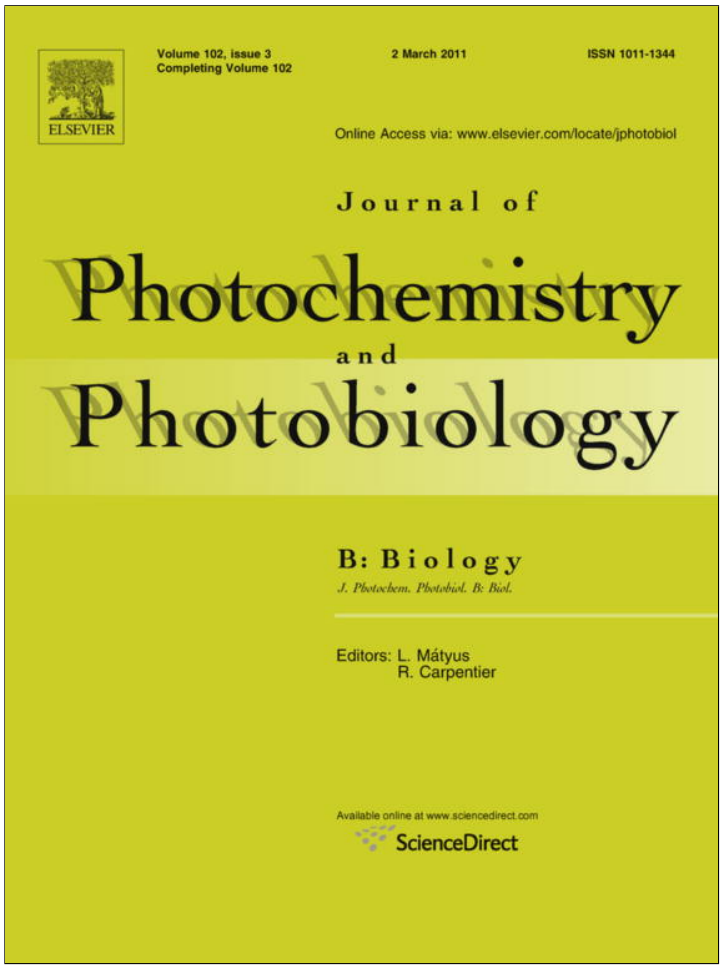

Journal of Photochemistry and Photobiology B: Biology 102 (2011) 209–217

Contents lists available at ScienceDirect

Journal of Photochemistry and Photobiology B: Biology

journal homepage: www.elsevier.com/locate/jphotobiol

UV and visible light screening by individual sporopollenin exines derived from *Lycopodium clavatum* (club moss) and *Ambrosia trifida* (giant ragweed)

Stephen L. Atkin [b,d], Sylvain Barrier [a,b], Zhenggang Cui [a], Paul D.I. Fletcher [a,*], Grahame Mackenzie [a,b], Vincent Panel [b], Vincent Sol [c], Xunli Zhang [a]

[a] Department of Chemistry, University of Hull, Hull HU6 7RX, UK
[b] Sporomex Ltd., Department of Chemistry, University of Hull, Hull HU6 7RX, UK
[c] Université de Limoges, Faculté des Sciences et Techniques, Laboratoire de Chimie des Substances Naturelles, 123 Avenue Albert Thomas, 87060 Limoges, France
[d] Hull York Medical School, Michael White Diabetes Centre, 220-236, Anlaby Road, Hull, HU3 2RW, UK

ARTICLE INFO

Article history:
Received 23 May 2010
Received in revised form 7 December 2010
Accepted 8 December 2010
Available online 21 December 2010

Keywords:
Sporopollenin
Plant spores
Pollen
Screening
UV–visible light transmission
UV–visible light absorbance

ABSTRACT

We have investigated the UV–visible light transmission of three types of micrometre-sized sporopollenin exine shells, two derived from *Lycopodium clavatum* (club moss) spores and one from *Ambrosia trifida* (giant ragweed) pollen. We have used spectrophotometer measurements of partial monolayers of exines and microscope absorbance imaging to derive the light transmission properties of *individual* exines. Measurements have been made for exines in air when light transmission losses are due to a combination of absorption, reflection and scattering processes and for exines dispersed in a liquid for which the refractive index (RI) is approximately equal to the RI of the exine such that reflection and scattering effects are negligible. Overall, it found that the light transmission of a single exine wall is approximately 50%. This value of the transmission is due mainly to light absorption, is similar for the three exines studied here and varies only slightly with light wavelength over the range 200–900 nm.

1. Introduction

Pollen grains of flowering plants and spores of non-flowering plants have a double-layered wall structure which protects their contents [1,2]. The intine is the inner wall and consists primarily of cellulose and other polysaccharides. The exine, the outer wall, consists mainly of sporopollenin and confers great resistance to biological decay and chemical attack [3]. Early work by Zetzsche et al. [4,5] led to the conclusion that sporopollenin is a mixture of unsaturated polymers composed of carbon, hydrogen and oxygen with an empirical formula of $C_{90}H_{144}O_{27}$ (for sporopollenin from *Lycopodium clavatum* with formula based on a C_{90} unit) and containing methyl and hydroxyl groups. Later investigations by Shaw and co-workers [6–10] suggested that sporopollenin is formed by oxidative polymerisation of carotenoids and carotenoid esters. More recently, it has been described as a mostly aliphatic polymer possessing aromatic units including *p*-coumaric and ferulic acids [11]. Also a putative structure consisting of an aliphatic framework possessing the coumaric and ferulic acid groups as side chains has been proposed in a review by van Bergen et al. [12].

Using suitable chemical treatments, it is possible to extract the "raw" spore or pollen to produce intact hollow shells consisting only of the sporopollenin exine coatings [3]. We have investigated the transmission of UV–visible light by these sporopollenin exine shells with the following main motivations in mind. Firstly, the sporopollenin exine shells can be used to encapsulate a variety of species including lipids, unsaturated oils and proteins [13] and it has been shown that sporopollenin-encapsulated species are protected from chemical degradation induced by UV-light exposure [14]. It is of interest to measure the transmission of UV–visible light through a single thickness of the exine shell in order to help understand the origin and magnitude of the light protection phenomenon. Secondly, Rozema et al. [15,16] investigated the UV-B absorbing compounds (UACs) in different components of pollen and spores from plants previously exposed to doses of UV-B light. Chemical analysis of UACs in the solvent-extractable, wall-bound and sporopollenin components revealed significant differences in compositions from plants with and without exposure to UV-B. The authors suggested that application of this method to old pollen and spore samples might be used for the reconstruction of the historic variation in solar UV-B levels. However, within the literature on sporopollenins [1–3,12] and ultraviolet radiation screening compounds (see, for example, the review by Cockell and Knowland [17]), to our knowledge, there are no direct measurements of the UV–visible spectra of individual sporopollenin exine shells.

* Corresponding author. Address: Surfactant & Colloid Group, Department of Chemistry, University of Hull, Hull HU6 7RX, UK. Tel.: +44 01482 465433; fax: +44 01482 466410.
E-mail address: P.D.Fletcher@hull.ac.uk (P.D.I. Fletcher).

1011-1344/$ - see front matter © 2010 Elsevier B.V. All rights reserved.
doi:10.1016/j.jphotobiol.2010.12.005

Rozema et al. [15] quote values of the relative UV-B absorbance (integrated over the wavelength range 280–320 nm) of suspensions of sporopollenin in glycerol. Uber [19] describes ultra-violet spectrophotometry of Zea Mays pollen with a quartz microscope. However, these results do not give information about the light screening effect of a single wall of a sporopollenin exine shell, i.e. the reduction in light transmission on passage from the outside to the inside of the shell. With this motivation in mind, the main objectives of this study are to make direct measurements of the UV–visible absorbance spectrum of single sporopollenin exine shells and to determine whether the light transmission methods using microscopy developed as part of this work can contribute to the elucidation of the physical structure of these particles.

2. Materials and methods

We have used three types of exines as shown in Fig. 1. The first, extracted from *L. clavatum* (club moss), are approximately 25 μm diameter and were obtained from Tibrewala International. The second type, also marketed as *L. clavatum* club moss, is approximately 40 μm in diameter and was obtained from Post Apple Scientific. The smaller form is reticulated whilst the larger is smoother and more rounded. These two types are abbreviated here as LC25 and LC40 respectively. The third type is from *Ambrosia trifida* (giant ragweed) and is approximately 15 μm in diameter. This was obtained from Sigma–Aldrich and is denoted here as AT15.

2.1. Extraction of exines

The sporopollenin exine shells were prepared as follows. Raw *L. clavatum* particles (loose powder, 250 g) were suspended in acetone (750 cm^3) and stirred under reflux for 4 h. The defatted sporopollenin (DFS) was filtered (porosity grade 4) and dried overnight in open air. The DFS was then suspended in 6% (w/v) potassium hydroxide aqueous solution (750 cm^3) and stirred under reflux for 6 h. After filtration (porosity grade 4), this operation was repeated with fresh 6% (w/v) potassium hydroxide solution (750 cm^3). The suspension was then filtered (porosity grade 4). The solid was washed with hot water (3×300 cm^3) and hot ethanol (2×300 cm^3), refluxed in ethanol (750 cm^3) for 2 h, filtered (porosity grade 4) and dried overnight in open air to yield base-hydrolysed sporopollenin (BHS). In order to remove the cellulose intine, the BHS was suspended in 85% (v/v) ortho-phosphoric acid (750 cm^3) and stirred under reflux for 7 days. The solid was filtered (porosity grade 4), washed with water (5×250 cm^3), acetone (250 cm^3), 2 M aqueous hydrochloric acid (250 cm^3), 2 M aqueous sodium hydroxide (250 cm^3), water (5×250 cm^3), acetone (250 cm^3) and ethanol (250 cm^3) and finally dried under vacuum over P_2O_5 or in an oven at 60 °C to give sporopollenin exines (LC25 or LC40) (58–60 g) accordingly.

Raw *A. trifida* pollen (loose powder, 5 g) was suspended in acetone (15 cm^3) and stirred under reflux for 1 h. The defatted sporopollenin (DFS) was filtered (porosity grade 5) and dried overnight in open air. The DFS was then suspended in 1% (w/v) sodium hydroxide aqueous solution (30 cm^3) and stirred under reflux for 1 h. After partial filtration (porosity grade 5), the suspension was neutralised with concentrated hydrochloric acid (5 cm^3), diluted in ethanol (up to 75 cm^3) then refluxed for 1 h, filtered (porosity grade 5) and dried overnight in open air. The resultant base-hydrolysed sporopollenin (BHS) was suspended in 85% (v/v) ortho-phosphoric acid (85 cm^3) and stirred under reflux for 1 h. The solid was diluted with ethanol (100 cm^3), filtered (porosity grade 5), washed with (1/1 (v/v)) water/ethanol (5×100 cm^3) and ethanol (100 cm^3) and dried under vacuum over P_2O_5 or in an oven at 60 °C to give sporopollenin exines (AT15) (1.2 g).

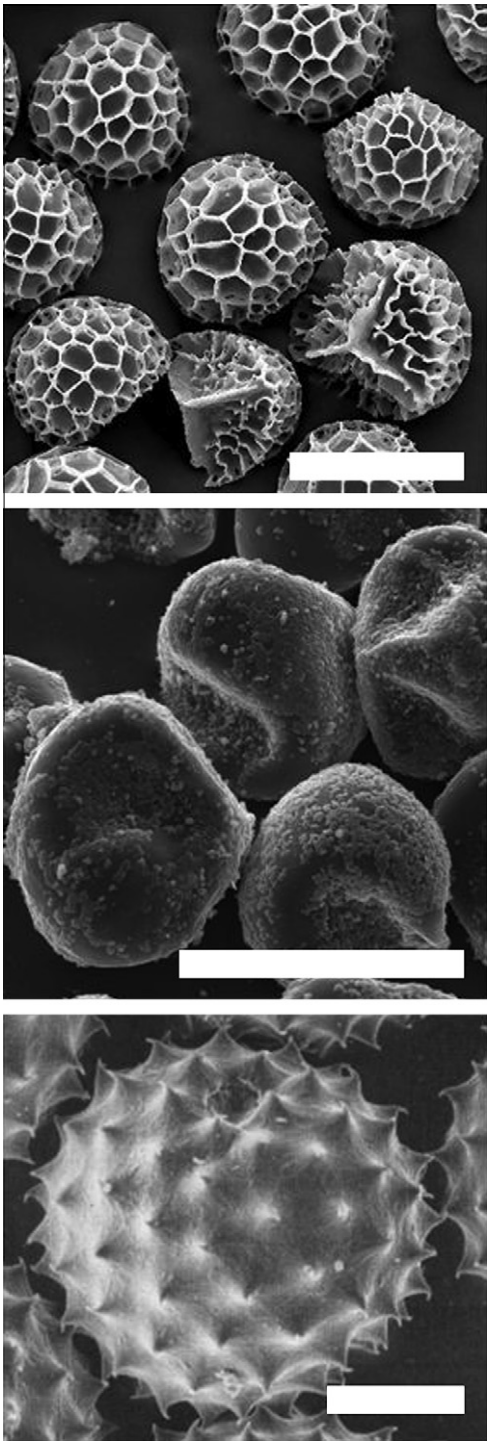

Fig. 1. Scanning electron micrographs of 25 μm diameter spores from *Lycopodium clavatum* (LC25) with scale bar = 25 μm(top image), 40 μm diameter spores from *Lycopodium clavatum* (LC40) with scale bar = 50 μm (middle image) and 15 μm pollen grains from *Ambrosia trifida* (AT15) with scale bar = 10 μm (bottom image).

CHN combustion analysis of the final extracted material, performed using a Fisons EA 1108 instrument, gave the results shown in Table 1. It can be seen that the values are consistent with literature values [3] of the empirical formulae for sporopollenins derived from different sources and that the final extracted exine shells contain either zero or only a trace of nitrogen-containing species.

Table 1
CHN combustion elemental analysis of the exines extracted from *Lycopodium clavatum* (club moss) spores (LC25 & LC40) and one from *Ambrosia trifida* (giant ragweed) pollen (AT15).

	LC25	LC40	AT15
wt.% C	58.3	60.6	69.4
wt.% H	7.1	7.0	9.3
wt.% N	0.0	0.0	1.8
wt.% O (by difference)	34.6	32.3	19.5

2.2. UV–visible transmission properties of individual exines

Two methods were used to determine the UV–visible transmission properties of the sporopollenin exine shells. For both methods, the overall light transmission is determined by a combination of light absorption, reflection and scattering processes. Light reflection and scattering is proportional to the square of the difference in refractive index (RI) of the exine and surrounding medium and so is significant for sporopollenin exines in air when the RI difference between the exine and surrounding medium is large. As reported in Ref. [20], sporopollenin exines are approximately refractive index matched to their surrounding fluid when dispersed in glycerol (RI = 1.475 [21]). Hence, light transmission of sporopollenin is expected to be determined almost entirely by absorption when the exines are dispersed in either glycerol or toluene (RI = 1.496 [21]) which both have RI values close to that of sporopollenin. Using both methods described below, optical transmission measurements were made both under air and dispersed in either glycerol or toluene in order to separate effects due to light absorption and reflection/scattering.

In the first method, the UV–visible spectra of partial monolayers of the exines were measured using a Unicam UV3 spectrophotometer. The exines were spread evenly over a quartz plate, either as a dry powder, from a dispersion in ethanol with subsequent evaporation of the solvent, or as a dispersion in glycerol or toluene. The cell was completed by attaching the upper quartz plate and fixing with plastic bands over the ends (see Fig. 2). For each sample preparation, care was taken to ensure the exine layer thickness did not exceed a single particle at any point; this was checked by examination under a microscope. In addition, the gap between the quartz plates was measured using a microscope focus method and found to be within approximately 10% of the outer diameter of the undistorted exines and hence it is likely that most exine shells are not significantly "squashed" when contained within the measurement cell. To record the spectra, the cell was taped in place in the sample position on the front of standard cuvette holder of the spectrophotometer. The exine monolayer sample spectrum was recorded vs. air and the exine spectrum obtained by subtraction of the separately recorded reference spectrum of the empty cell containing only air or glycerol, again vs. air. In addition to the spectrum, the area fraction occupied by the exine monolayer within the cell was determined by recording an optical transmission micrograph image using an Olympus BX51 microscope. The fractional area occupied by the exines was derived from the images using Image-Plus Pro software. The theoretical analysis used to derive the absorbance properties of the individual exines from the measured sets of spectra of the exine partial monolayers covering a range of exine area fraction is detailed in Appendix A.

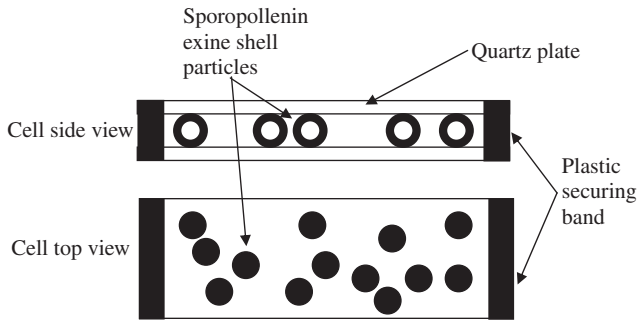

Fig. 2. Schematic of the cell used to measure the light transmission spectra of the partial monolayers of sporopollenin exine shells.

In the second method, we have used absorbance imaging based on transmission microscopy to obtain spatially resolved absorbance "maps" of the exines at a single fixed wavelength of 450 nm. This method, originally developed to determine channel dimensions in "Lab-on-a-chip" microchannel devices and used to characterise emulsions stabilised by adsorbed films of light absorbing carbon black particles, is fully detailed in Refs. [22,23]. An inverted transmission microscope equipped with a digital camera and a narrow bandpass filter allowing light transmission at a wavelength of 450 nm is used to obtain three images, each consisting of an array of individual pixel light intensity values. The first image is recorded with a partial monolayer of sporopollenin exine shells on a glass slide. This image yields an array of pixel transmitted intensities denoted I. A second image under identical conditions but in the absence of the exines yields the pixel intensity array I_0 corresponding to the incident light intensity on each pixel. The third image, recorded in the absence of sample exines and with the microscope light blanked off, yields the intensity array denoted I_{dark} which is recorded to correct for the "dark" signal of the camera. The three intensity arrays are then combined using Microsoft Excel to give the final array of pixel-by-pixel absorbance values A_{pixel} making up a so-called "absorbance image" according to

$$A_{pixel} = \log_{10}\left(\frac{I_0 - I_{dark}}{I - I_{dark}}\right) \quad (1)$$

Microscopic absorbance images of monolayer exine samples, prepared as described above, were obtained using a Zeiss Axiovert transmission inverted microscope with a 10× objective lens at a single wavelength of 450 nm. The pixel size in the recorded image sets was 1.596 × 1.596 μm.

2.3. Confocal fluorescence and electron microscopies

Confocal images were obtained using a Bio-Rad Radiance 2100 laser scanning confocal microscope (LSCM) equipped with Ar (488 nm), Green HeNe (563 nm) and Red diode (637 nm) laser excitation and connected to a Nikon TE-2000E inverted microscope. Images were collected using Lasersharp2000 software under the following conditions; laser excitation lines Ar (488 nm) 15%, Red diode (637 nm) 38%, fluorescence from samples passed through 560 and 650 nm dichroic filters and was collected in photomultiplier tubes (PMT) equipped with the following emission filters, 515/30, 590/70 and 600 long pass. The laser scan speed was set at 166 lines per sec, and the viewable area was between 20 and up to 200 mm^2 when using a 60× oil objective. No fluorescent dyes were added to the sporopollenin samples; the emission collected originated from fluorophores indigenous to the sporopollenin exines [24].

Samples for SEM of dry pollen or spores and the exines derived from them were prepared by pressing sample mount containing a self-adhesive carbon disk into a mound of the powder. Excess loose particles were removed with compressed air. The sample mount was then coated with a thin (approximately 10 nm) layer of carbon

in an Edwards vacuum evaporator and SEM images obtained using a Cambridge Instruments 360SEM.

All measurements were made at room temperature of 20 ± 2 °C.

3. Results and discussion

The appearance of the original spores and pollens are shown in Fig. 1. Fig. 3 shows confocal fluorescence microscope images of the original particles and the extracted sporopollenin exines of LC25 which were obtained using the intrinsic fluorescence of the exine material. The latter image shows an internal void and an outer surface which appears undamaged in comparison with the untreated LC25. The exine wall has a thickness (not including the pattern of exterior ridges) of 2–3 μm with the layer of ridges being of similar dimension. Using similar images for the other exines (not shown), the wall thicknesses of LC40 and AT15 were also estimated to be 2–3 μm. It should be noted that these estimates of the wall thickness refer to those parts which contain the intrinsic fluorophores responsible for the fluorescence signal. The possibility of "dark" non-fluorescent regions cannot be excluded.

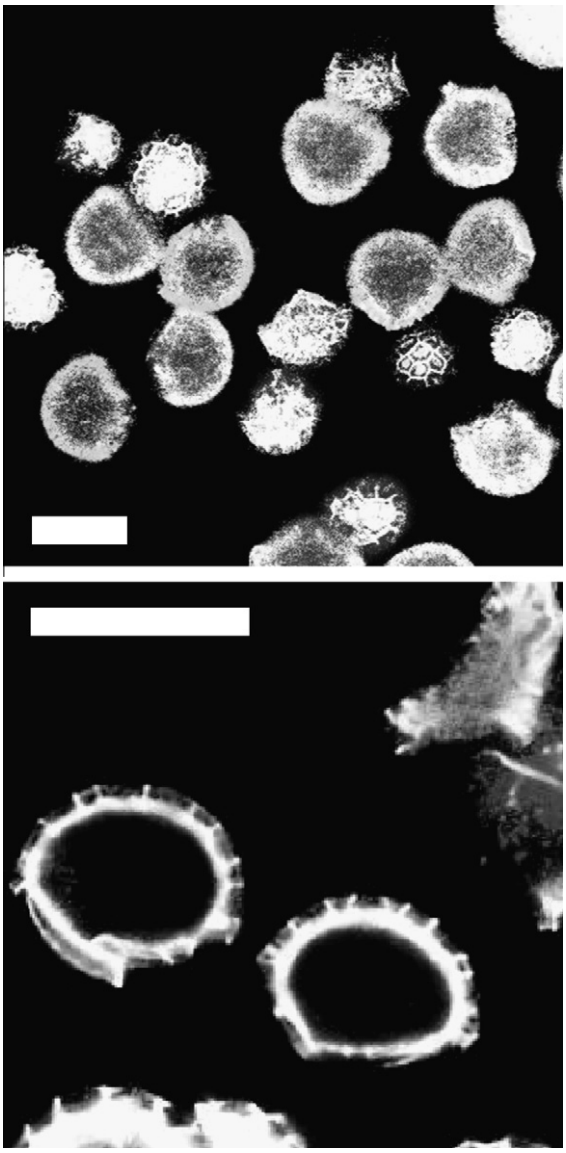

Fig. 3. Confocal fluorescence micrographs of LC25. The top image shows the untreated particles still containing their natural contents and the lower image shows the empty sporopollenin exine shells. The scale bars correspond to 25 μm in each image.

3.1. Spectra of partial monolayers of sporopollenin exines

Optical transmission spectra were measured over the wavelength range 190–900 nm for partial monolayers of the three types of sporopollenin exines, both under air (where the derived absorbance values may contain significant contributions from absorption, reflection and scattering) and under glycerol where the approximate RI-matching means that the derived absorbance values correspond to light absorption only.

For each wavelength, the data of measured absorbance A_{meas} as a function of the exine area fraction A_f were used to derive the value of A, equal to the average absorbance of the area fraction occupied by exines, according to Eq. (A3) in Appendix A. The validity of Eqs. (A2) and (A3) was tested by comparing the predicted and measured variation of absorbance A_{meas} (averaged over the entire wavelength range 190–900 nm) with A_f. Fig. 4 shows the comparison of the experimental data for all three exine types dispersed in glycerol with the behaviour predicted by Eq. (A2) (solid line) with the (wavelength averaged) value of A set to 0.80. The good agreement between the measured and calculated data confirms the validity of Eq. (A2) and also shows that the transmission properties of the three different exine types are very similar. Data sets for the different exine types in air (not shown) showed similar behaviour but with slightly higher values of A, due to the additional loss of optical transmission caused by reflection and scattering.

The final derived spectra (i.e., A values vs. wavelength) for the three exine types in air and in glycerol are shown in Fig. 5 as 3rd-order polynomial fitted lines. The overall conclusions are: (i) that, with the exception of the small maxima seen for LC40, the absorbance is almost independent of wavelength; (ii) the spectra and absolute absorbance values are very similar for the three particles types; (iii) the full monolayer absorbance values in air (with contributions from absorption, reflection and scattering) are approximately 10% higher than the values in the RI-matching solvent glycerol where the absorbance is due only to light absorption.

To estimate the absorbance and corresponding transmission of a single exine shell thickness and the absolute value of extinction coefficient ε, we must first estimate the average optical path length corresponding to the measurement of A which is an average over all the area occupied by shell particles $\bar{x}$. As noted above, the measured thicknesses of the partial monolayers (i.e. the gap in the sample cell) were all within 10% of the undistorted diameters of the particles and hence are considered unlikely to be "squashed"

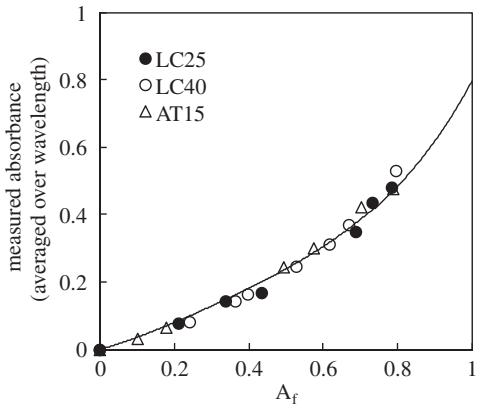

Fig. 4. Measured absorbance (averaged over wavelengths 200–900 nm) plotted vs. area fraction A_f for partial monolayers of the three exine types in glycerol. The solid line is calculated using Eq. (3) with the value of A equal to 0.80.

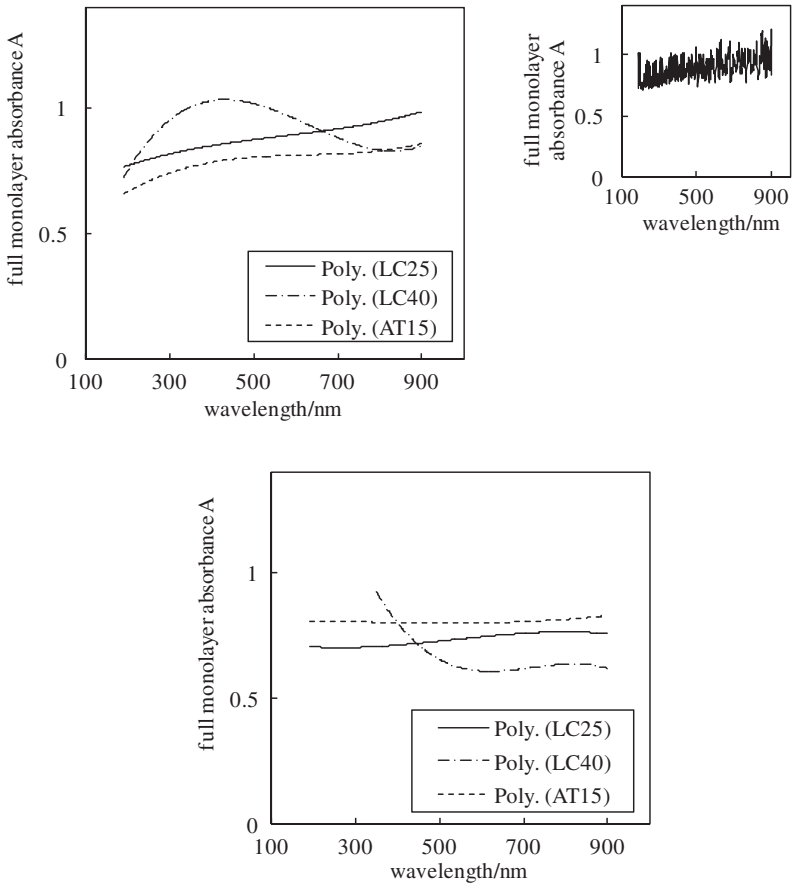

Fig. 5. Derived values of full monolayer absorbance *A* vs. wavelength for the three exine types in air (upper plot) and in glycerol (lower plot). The plots are shown as smooth, 3rd-order polynomial fits to the curves in order to improve the clarity of the figure. The root mean-square error between the polynomial fits and the derived data of *A* vs. wavelength (see inset plot for LC25 in air) is 0.07 for LC25 in air and similar for the other exines.

by confinement within the cell. Hence, it is expected that $\bar{x}$ should lie between $4t/3$ and $4t$, depending on the ratio of inner radius r to wall thickness t (Eq. (A5) in Appendix A). We assume the wall thickness t to be 3 μm for all particles (as indicated by the confocal microscope images) and take the outer radii to be 25, 40 and 15 μm for LC25, LC40 and AT15 respectively. As shown in Table 2, this enables the estimation of the absorbance and corresponding% transmission of a single exine shell and the absorption coefficient ε for the different particles in air and in RI-matching solvent. It can be seen that the% transmission at a wavelength of 450 nm (but which is similar for all wavelengths) is in the range 38–51% in air and higher (38–61%) in glycerol. The assumption that the wall thickness is 3 μm for all samples gives values of the absorption coefficient which are around 0.1 μm^{-1}.

Table 2
Comparison of overall absorbance, single-wall absorbance and transmission and absorption coefficient for LC25, LC40 and AT15 exines in air and dispersed in an RI-matching solvent (glycerol or toluene). All values refer to a wavelength of 450 nm.

Sample	*A* at 450 nm	$\bar{x}/t$	A for 1 wall thickness	% transmission	$\varepsilon/\mu m^{-1}$ (t/μm)
Absorbance of partial monolayers					
LC25 in air	0.86	2.9	0.30	51	0.10 (3)
LC40 in air	1.02	3.3	0.31	49	0.10 (3)
AT15 in air	0.80	1.9	0.42	38	0.14 (3)
LC25 in glycerol	0.72	2.9	0.25	56	0.08 (3)
LC40 in glycerol	0.72	3.3	0.22	61	0.07 (3)
AT15 in glycerol	0.81	1.9	0.42	38	0.14 (3)
Absorbance imaging					
LC25 in air	0.55[a]	2	0.28	53	0.02 (12.5)
LC40 in air	0.65[a]	2	0.33	47	0.02 (20)
AT15 in air	0.55[a]	2	0.28	53	0.04 (7.5)
LC25 in toluene	0.40[a]	2	0.20	63	0.03 (6)
LC40 in toluene	0.45[a]	2	0.23	60	0.02 (10)
AT15 in toluene	0.18[a]	2	0.09	81	0.02 (5)

[a] These absorbance values are measured through the poles of the shell particles where x/t = 2.

Some limited comparisons can be made between the spectral parameters measured here and literature data. Based on data from Refs. [17,18] and referring to *Brassica rapa*, Rozema et al. [15], state "The pollen wall is effective in screening out more than 80% of the incident UV radiation". Spectra of glycerol suspensions of sporopollenin derived from different microscopic algae have been measured [20]. Although the results show the shape of the spectra, they do not yield the absolute values of the absorption coefficient. For these various algae sporopollenins, the absorbance values depend strongly on the alga type but the wavelength dependences are rather similar; the absorbance simply decreases progressively with increasing wavelength from 280 to 700 nm [20]. The value of the absorption coefficient ε for these sporopollenin shells can be compared with that for carbon black particles as used in inks. The spectrum of carbon black particle suspensions is very similar to that for the algal-derived sporopollenin from Ref. [20], the absorbance progressively and smoothly decreases with wavelength from 190 to 900 nm and the absorption coefficient is 1.6 μm^{-1} at 450 nm [23], more than 1 order of magnitude higher than the values estimated here for sporopollenin. We speculate here that the different absolute magnitudes of the absorption coefficients may reflect the relative amounts of large, delocalised aromatic species with sp2 hybridised carbon atoms and the sp3 carbon content in sporopollenin [11,12,3] compared to carbon black.

3.2. Absorbance imaging of sporopollenin exine shells

Fig. 6 shows an example of an optical transmission micrograph at wavelength of 450 nm of a partial monolayer of LC40 exine shells in toluene together with the derived pixel-by-pixel absorbance image. The non-spherical LC40 exines in the partial monolayer are randomly oriented which results in the derived absorbance images of the different particles in the lower image having different shapes. Despite this variability between individual exines in the image, it can be seen that the overall absorbance values are reasonably consistent with the values shown in Fig. 5. In Fig. 7, a cross-section through the centre of the absorbance image of a single exine from Fig. 6 is compared with a profile calculated for a hypothetical, spherical shell in which the thickness and absorption coefficient of the wall is uniform (Eq. (5)). For this particular exine (corresponding to one random orientation in the sample cell), the cross-section has the characteristic double maximum profile expected for a hollow shell. However, it should be noted that the parameters of the calculated profile (shown in the figure legend) correspond to a shell wall thickness of 10 μm, considerably higher than that estimated from the confocal images of Fig. 3 (about 3 μm). The simulated outer diameter of the exine, equal to twice $(r + t)$, of 44 μm is close to the average outer diameter of LC40 exines estimated from electron microscope images (40 μm). The fact that the fitted profile yields a higher value of t than that estimated from the confocal microscopy also means that the value of absorption coefficient ε derived from the absorbance imaging is correspondingly lower than from the exine partial monolayer absorbance results.

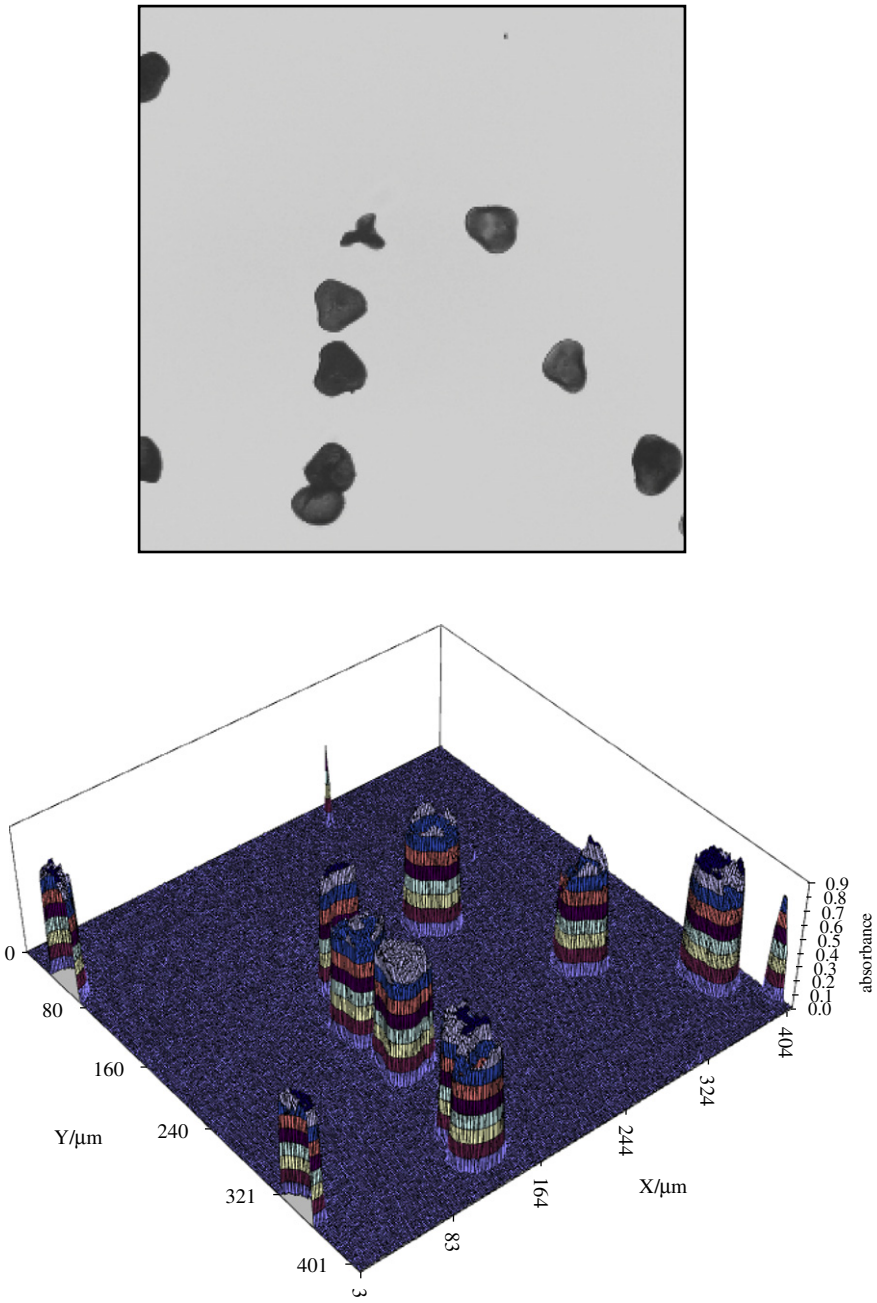

Fig. 6. LC40 sporopollenin exine shells in toluene recorded using a 10× objective lens and 450 nm filter. The upper image shows the optical transmission image and the lower plot shows the derived pixel-by-pixel absorbance image.

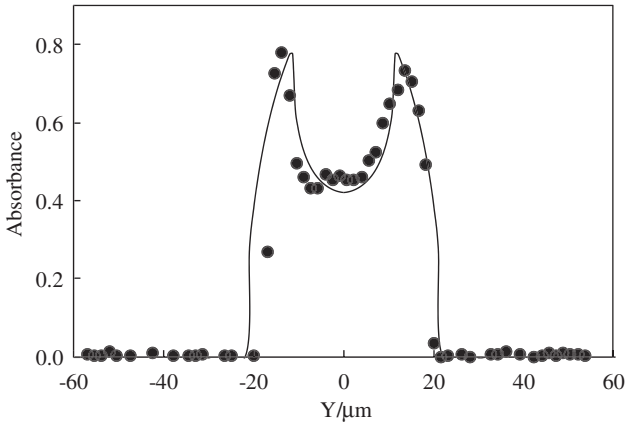

Fig. 7. A "slice" through the absorbance image of one example of a single LC40 sporopollenin exine shell particle in toluene recorded using a 10× objective lens and 450 nm filter. For comparison, the solid line shows a theoretical profile calculated for a (hypothetical) spherical shell of inner radius 12 μm, wall thickness 10 μm and extinction coefficient 0.021 μm^{-1} for which the shell has uniform thickness and extinction coefficient.

The absorbance images of all three exine types dispersed in the RI-matching solvent toluene show similar behaviour. Although there is significant variability between individual exines due to random orientation, most particle profiles have absorbance values which are approximately consistent with those of Fig. 5 and show the double-maxima shape (as seen for the example particle of Fig. 7) which is characteristic of hollow shells. As in Fig. 7, attempts to fit these profiles to a uniform thickness, spherical shell model generally suggest shell wall thicknesses larger than those estimated from the confocal microscope images of Fig. 3. The origin of this discrepancy currently remains unclear but could be a consequence of the distributions of the intrinsic fluorophore species (used to obtain the confocal images) and the absorbing species (used in these absorbance images) within the exine shells being non-identical. It might also be a consequence of a significant fraction of the exines forming "deflated" shell structures rather than annular spherical shells. In principle, some distortion of the absorbance image profiles may result from the angular distribution of the incident light in the transmission microscopy. This putative explanation is less likely since, as discussed in Ref. [22], artefacts due to this effect are minimised by use of the low (10×) magnification objective lens and absorbance image results for RI-matched emulsions stabilised by shells of light absorbing carbon black particles generally show good fits to the uniform shell model [23].

Representative absorbance images of the different exine types in air are shown in Fig. 8. Under air, the exines' optical transmission is reduced owing to reflection and scattering processes. This effect causes the absorbance images of the exines to be more "rounded" than for the exines in an RI-matching solvent, i.e. the double maxima in the absorbance cross sectional profiles are less pronounced or absent altogether, indicating again that the wall thicknesses are larger than 3 μm.

The overall absorbance (measured through the poles of the exines), the single-wall transmission values and the absorption coefficients derived from absorbance images are summarised and compared with those from partial monolayers in Table 2. With the exception of AT15, there is reasonable agreement for the single-wall transmission values between the two methods. The origin of the discrepancy, particularly for AT15 in RI-matching solvents, is presently unclear but might possibly be related to the use of toluene in one case and glycerol in the other as the dispersion medium which appears to cause the unexpected differences in values only for the case of AT15. The values of the absorption coefficient ε

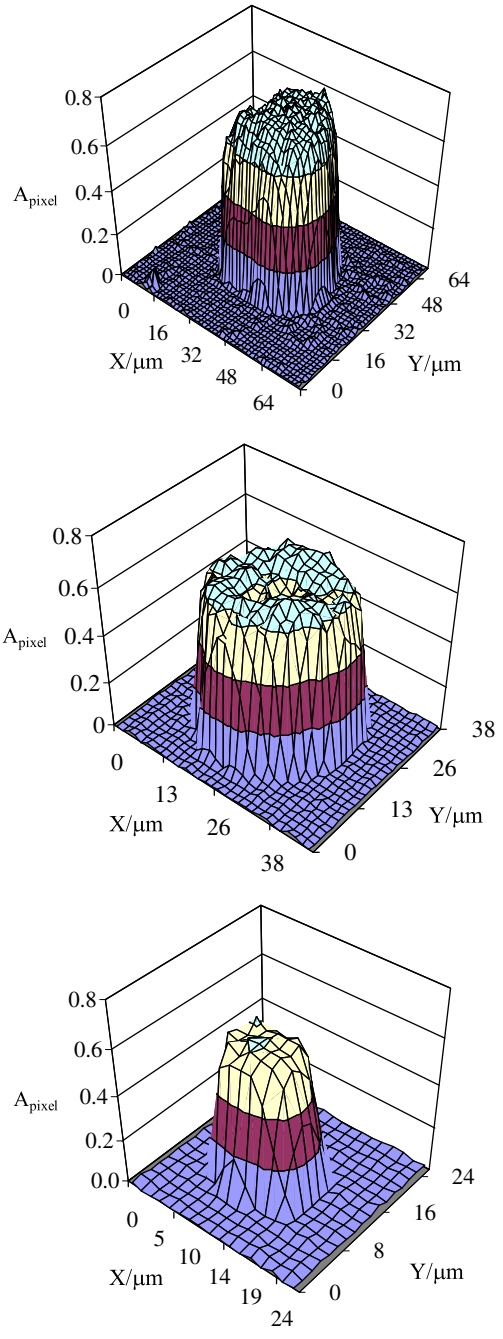

Fig. 8. Examples of absorbance images recorded at 450 nm with a 10× objective lens for LC40 (upper image), LC25 (middle image) and AT15 sporopollenin exine shells (lower image) in air.

estimated from absorbance imaging are significantly lower than those estimated from the partial monolayer results. This is primarily a consequence of the assumption that $t = 3$ μm (from confocal microscopy) was used for the partial monolayers whereas t was independently estimated by fitting the shapes of the absorbance image profiles (e.g. Fig. 7 and the figures in parentheses in the final column of Table 2). The results indicate that the light absorbing material of the exine shells is distributed over wall thicknesses which are larger than the 3 μm indicated by the confocal microscopy images and that a more realistic absorption coefficient of the sporopollenin material is near to 0.02 μm^{-1}. The larger than expected wall thicknesses observed here may be a consequence of some fraction of the exines having the form of "deflated" shells.

4. Conclusions

We have used spectrophotometric measurements of partial monolayers of sporopollenin exines to estimate the UV–visible absorption spectra and absolute absorption coefficients of individual exines derived from *L. clavatum* (club moss) and *A. trifida* (giant ragweed). Relevant to the use of such exines for encapsulating material, it is found that the light transmission of a single sporopollenin exine wall thickness is approximately 50% and shows only minor variation with the type of particle and the wavelength over range 200–900 nm (Table 2). Comparison of the spectra of the exines in air and dispersed in an RI-matching solvent reveal that optical losses due to reflection and scattering processes are relatively minor in comparison with those due to light absorption. The absolute values of the light absorption coefficients (based on a particle wall thickness of 3 μm) are of the order of 0.1 μm^{-1}. The methodology developed here and the spectral information may aid the development of the use of analysis of old pollen and spore samples to reconstruct the historic variation in solar UV-B levels.

In addition, we have used a absorbance imaging method based on light transmission microscopy at a single incident wavelength (450 nm) to provide independent measurements of the spectral parameters at this single wavelength and to elucidate the physical structure of the exines. Using this method, the average wall thicknesses of the exines are found to be larger than those estimated using confocal fluorescence microscopy. Both absorbance imaging and partial monolayer spectrophotmetry yield similar values for the% light transmission of a single sporopollenin exine wall. However, because of the different estimated wall thicknesses used, the light absorption coefficients estimated from the absorbance images (approx. 0.02 μm^{-1}) are lower than values from the partial monolayer method (approx. 0.1 μm^{-1}).

Acknowledgements

We thank Dr. John Clint of the Department of Chemistry, University of Hull for helpful discussions and Ms. Carole Kennedy, Department of Chemistry, University of Hull for making the C, H, and N analyses.

Appendix A. Theory of optical transmission spectra of partial monolayers of sporopollenin exine shells

The absorbance A due solely to light absorption of a solid material varies with its thickness x according to

$$A = \log_{10}\frac{I_0}{I} = -\log_{10}T = \varepsilon x \tag{A1}$$

where I_0 and I are the incident and transmitted light intensities, T is the transmission and ε is the absorption coefficient equal to the absorbance per unit length travelled by the light *within the solid material*. A sample consisting of a partial monolayer of exines, as shown schematically in Fig. 2, contains an area fraction A_f covered with particles of transmission T and absorbance A plus an area fraction $(1 - A_f)$ with 100% transmission corresponding to $A = 0$. In this situation, the overall measured absorbance A_{meas} of the partial monolayer of exines is determined by the absorbance of an individual exine (A) and the area fractional coverage (A_f) according to:

$$A_{meas} = -\log_{10}[A_f 10^{-A} + (1 - A_f)] \tag{A2}$$

and hence

$$A = \varepsilon x = -\log_{10}\left[\frac{10^{-A_{meas}}}{A_f} + \frac{A_f - 1}{A_f}\right] \tag{A3}$$

Using measurements of A_{meas} as a function of A_f, Eq. (A3) enables the estimation of A, equal to the mean absorbance of a single exine averaged over the projected area of the exine. Deriving the true extinction coefficient ε requires knowledge of the distance x travelled by the light through the actual substance of the sporopollenin exine. For exines consisting (in their undistorted state) of spherical shells with inner radius r and with uniform thickness t, the value of x is a function of the equatorial distance from the centre of the particle a according to

$$\begin{aligned} x &= 2\left(\sqrt{(r+t)^2 - a^2} - \sqrt{r^2 - a^2}\right) && \text{for } 0 < a < r \\ x &= 2\left(\sqrt{(r+t)^2 - a^2}\right) && \text{for } r < a < (r+t) \\ x &= 0 && \text{for } (r+t) < a \end{aligned} \tag{A4}$$

The projected area average of x over the entire exine area is given by

$$\bar{x} = \frac{4}{3}\left(\frac{(r+t)^3 - r^3}{(r+t)^2}\right) \tag{A5}$$

Eq. (A5) has a limiting value of $4t/3$ as r tends to zero (i.e. a solid sphere) and $4t$ in the limit that $t \ll r$, corresponding to the case of a hollow, thin-walled sphere. For the same shell particle squashed flat, the particle would have a circular projected shape of almost uniform thickness equal to $2t$.

References

[1] K. Faegri, J. Iversen, Textbook of Pollen Analysis, Blackwell, Oxford, UK, 1964. p. 2.
[2] G. Shaw, in: J.B. Harborne (Ed.), Phytochemical Phylogeny, Academic Press, London, UK, 1970, pp. 31–35.
[3] G. Shaw, in: J. Brooks, P.R. Grant, M. Muir, P. Van, Gijzel, G. Shaweds (Eds.), Sporopollenin, Academic Press, London, New York, 1971, pp. 305–348.
[4] F. Zetzsche, K. Huggler, Untersuchungen über die Membran der Sporen und Pollen. I. 1. *Lycopodium clavatum*, L. Annalen 461 (1928) 89.
[5] F. Zetzsche, O. Kalin, Untersuchungen über die Membran der Sporen und Pollen V. 4. Zur Autoxydation der Sporopollenine, Helv. Chim. Acta 14 (1931) 517–519.
[6] J. Brooks, G. Shaw, Chemical structure of the exine of pollen walls and a new function for carotenoids in nature, Nature 219 (1968) 532.
[7] J. Brooks, G. Shaw, Identity of sporopollenin with older kerogen and new evidence for the possible biological source of chemicals in sedimentary rocks, Nature 220 (1968) 678–679.
[8] J. Brooks, G. Shaw, Evidence for extraterrestrial life: identity of sporopollenin with the insoluble organic matter present in the orgueil and murray meteorites and also in some terrestrial microfossils, Nature 223 (1969) 745–746.
[9] J. Brooks, G. Shaw, Relationship of kerogen and sporopollenin—a reply, Nature 227 (1970) 195–196.
[10] G. Shaw, A. Yeadon, Chemical studies on the constitution of some pollen and spore membranes, Grana Palynologica 5 (1964) 247–252.
[11] A. Meuter-Gerhards, C. Schwerdtfeger, S. Steuernagel, S. Wilmesmeier, R. Wiermann, Studies on sporopollenin structure during pollen development Zeitschrift Für Naturforschung C, J. Bioscience 50 (7–8) (1995) 487–492.
[12] P.F. van Bergen, P. Blokker, M.E. Collinson, J.S. Sinninghe Damsté, J.W. De Leeuw, Structural biomacromolecules in plants: what can be learnt from the fossil record?, in: A.R. Hemsley, I. Poole (Eds.), The Evolution of Plant Physiology. From Wholes Plants to Ecosystems, Elsevier, Academic Press, London, 2004, pp. 133–154.
[13] G. Mackenzie, S.T. Beckett, S. L. Atkin, Dosage form Comprising an Exines Coating of Sporopollenin or Derivatised Sporopollenin, Patent WO-2005/000280.
[14] G. Mackenzie, S.T. Beckett, S.L. Atkin, Uses of Sporopollenin: Antioxidant Properties of Sporopollenin Exines, Patent WO-2007/012856.
[15] J. Rozema, R.A. Broekman, P. Blokker, B.P. Meijkamp, N. de Bakker, J. van de Staaij, A. van Beem, F. Ariese, S.M. Kars, UV-B absorbance and UV-B absorbing compounds (para-coumaric acid) in pollen and sporopollenin: the perspective to track historic UV-B levels, J. Photochem. Photobiol. B 62 (2001) 108–117.
[16] J. Rozema, A.J. Noordijk, R.A. Broekman, A. van Beem, B.M. Meijkamp, N.V.J. de Bakker, J.W.M. van de Staaij, M. Stroetenga, S.J.P. Bohncke, M. Konert, S.M. Kars, H. Peat, R.I.L. Smith, P. Convey, (Poly)phenolic compounds in pollen and spores of Antarctic plants as indicators of solar UV-B: a new proxy for the reconstruction of past solar UV-B, Plant Ecol. 154 (2001) 11–26.
[17] C.S. Cockell, J. Knowland, Ultraviolet radiation screening compound, Biol. Rev. 74 (1999) 311–345.
[18] T.A. Day, S.M. Demchik, Ultraviolet-B radiation screening effectiveness of reproductive organs in *Hesperis matronalis*, Environ. Exp. Biol. 36 (1996) 447–454.

[19] F.M. Uber, Ultra-violet spectrophotometry of zea mays pollen with the quartz microscope, Am. J. Botany 26 (1939) 799–807.
[20] F. Xiong, J. Kemenda, J. Kopecky, L. Nedbal, Strategies of ultraviolet-B protection in microscopic algae, Physiol. Plantarum 100 (1997) 378–388.
[21] Handbook of Chemistry and Physics, Chemical Rubber, 62nd ed., Company Press, Boca Raton, 1981.
[22] I. Broadwell, P.D.I. Fletcher, S.J. Haswell, T. McCreedy, X. Zhang, Quantitative 3-dimensional profiling of channel networks within transparent lab-on-a-chip microreactors using a digital imaging method, Lab on a Chip 1 (2001) 66–71.
[23] B.P. Binks, Z.-G. Cui, P.D.I. Fletcher, Optical microscope imaging of carbon black nanoparticle films at solid and liquid interfaces, Langmuir 22 (2006) 1664–1670.
[24] G. Van Gijzel, in: J. Brooks, P.R. Grant, M. Muir, P. Van, Gijzel, G. Shaw (Eds.), Sporopollenin, Academic Press, London and New York, 1971, pp. 659–685.